iScience

CellPress
OPEN ACCESS

Article

Single-cell RNA-seq reveals a resolving immune phenotype in the oral mucosa

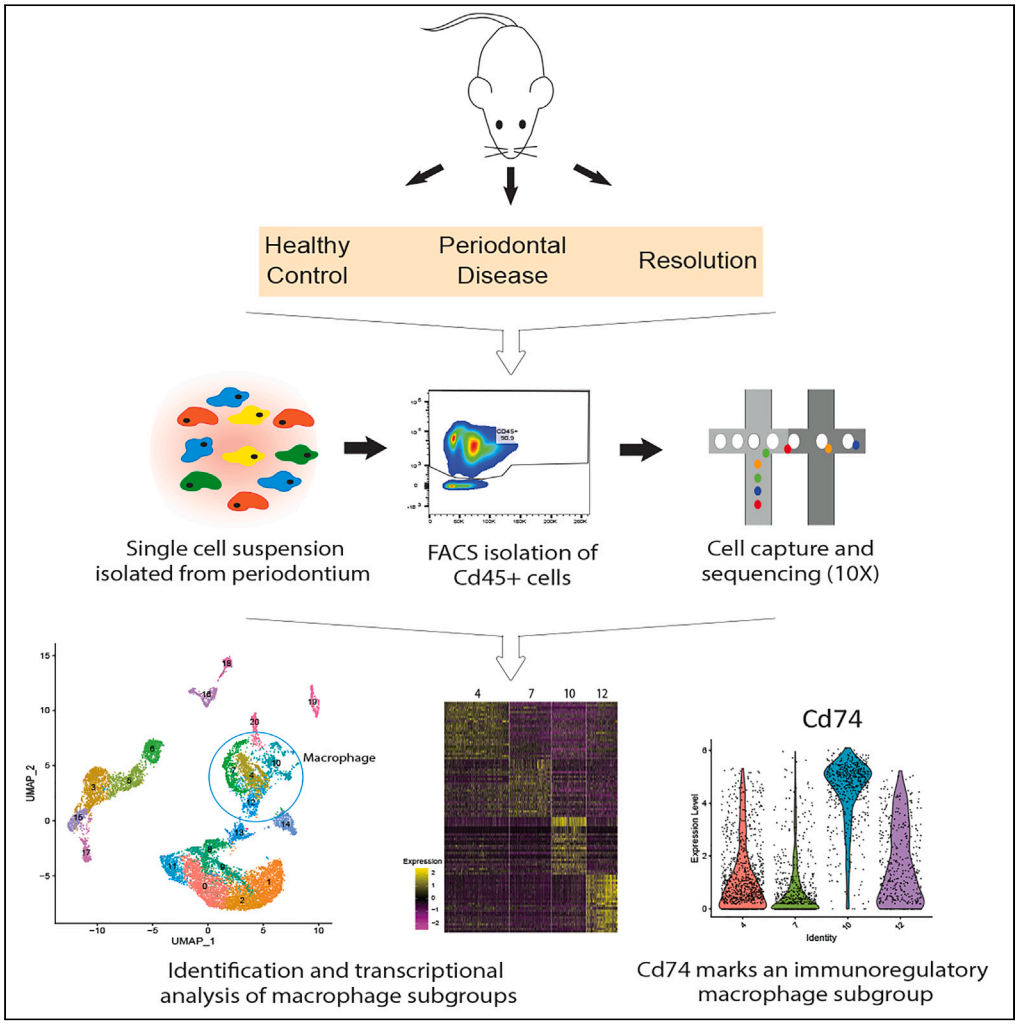

Paul Cantalupo, Alex Diacou, Sangmin Park, ..., Deshawna Glenn, Uma Chandran, Daniel Clark

daniel.clark@pitt.edu

Highlights

Resolution of periodontitis was modeled in mice and characterized via scRNA-seq

Macrophage subgroups differentially expand in health, disease, and resolution

Cd74 marks immunoregulatory macrophages associated with resolution of periodontitis

Cantalupo et al., iScience 27, 110735
September 20, 2024
https://doi.org/10.1016/j.isci.2024.110735

iScience

CellPress
OPEN ACCESS

Article

Single-cell RNA-seq reveals a resolving immune phenotype in the oral mucosa

Paul Cantalupo,[1] Alex Diacou,[2] Sangmin Park,[2] Vishal Soman,[1] Jiamiao Chen,[2] Deshawna Glenn,[2] Uma Chandran,[1] and Daniel Clark[2,3,4,*]

SUMMARY

The oral mucosa is the interface between the host immune response and the oral microbiota. In periodontal disease, the microbial plaque elicits a tissue-destructive immune response. Removal of the microbial stimulus initiates active resolution of inflammatory. Here, we use single-cell RNA-sequencing (scRNA-seq) to characterize the immune response within the oral mucosa across three distinct conditions of periodontal health, disease, and resolution in mice. We report gene expression shifts across the three conditions are driven by macrophage and neutrophils and identify a unique gene signature that characterizes resolution of disease. Macrophage subgroups are identified that demonstrate differential expansion across conditions, including a subgroup that expands during resolution with an immunoregulatory gene signature and enriched for surface marker Cd74. We validate expansion of this subgroup during resolution via flow cytometry. This work presents a robust single-cell dataset of immunological changes in the oral mucosa and identifies a resolution-associated macrophage phenotype in mucosal immunity.

INTRODUCTION

Periodontal disease is a chronic inflammatory condition that affects the supporting tissues of the teeth, eventually leading to tooth loss. Periodontal health is dependent on a symbiotic balance of the mucosal immune response with the oral microbiota. When pathologic shifts of the microbial plaque occur, qualitative and quantitative changes of the cellular immune response are evident.[1] The initial innate immune response in periodontal disease is characterized by neutrophil and macrophage infiltration followed by an adaptive immune response.[2,3] Eventual recruitment and activation of osteoclasts and matrix metalloproteinase activity leads to the tissue destruction surrounding teeth that is evident in periodontal disease.[4]

Removal of the pathologic microbial plaque eliminates the immune response stimulus, and the process of inflammatory resolution begins to promote the return to tissue homeostasis.[5] A timely and complete resolution of inflammation is necessary to limit the tissue damage. Resolution of inflammation is an active process that consists of the production of mediators that inhibit further immune cell recruitment, upregulation of apoptosis and efferocytosis, and initiation of the cascade of regenerative processes to repair damaged tissue.[6–8] Resolution of inflammation during periodontal disease is also characterized by phenotypic changes of immune cells. Multiple cellular phenotypes of macrophages, T cells, and neutrophils have been reported within the oral mucosa in conditions of periodontal health versus disease.[9–11] High-throughput transcriptional analysis has further led to the characterization of many diverse phenotypes that are tissue and disease specific.[12–14] However, less is understood about the immune cell phenotypes that actively drive inflammatory resolution.

The goal of this work was to demonstrate the unique cellular immune response across three distinct conditions of periodontal health, disease, and resolution in mice using single-cell RNA-sequencing (scRNA-seq). Here, we present the transcriptional signatures and cellular subgroups that characterize each condition and identify the differential gene regulation that defines that transition within the oral mucosa from health to disease and from disease to resolution. Interestingly, we identified significant diversity of macrophage populations within the oral mucosa. We characterized a transcriptionally distinct macrophage subgroup that expanded during the resolution condition and demonstrated an immunoregulatory gene signature. We identified a cell surface marker for this resolution-associated macrophage subgroup (Cd74) and validated the expansion of this subgroup during resolution via flow cytometry. These findings begin to identify markers of inflammatory resolution in periodontal disease to determine earlier and more accurate markers of disease progression versus resolution in the oral mucosa.

[1]Department of Biomedical Informatics, University of Pittsburgh School of Medicine, 5607 Baum Boulevard, Pittsburgh, PA 15206-3701, USA
[2]Center for Craniofacial Regeneration, University of Pittsburgh School of Dental Medicine, 335 Sutherland Dr., Pittsburgh, PA 15213, USA
[3]Department of Periodontics and Preventive Dentistry, University of Pittsburgh School of Dental Medicine, 3501 Terrace Street, Pittsburgh, PA 15213, USA
[4]Lead contact
*Correspondence: daniel.clark@pitt.edu
https://doi.org/10.1016/j.isci.2024.110735

RESULTS

Resolution of periodontal disease models a return to tissues homeostasis

We utilized a ligature model in mice to study the immune response across conditions of periodontal health (control), periodontal disease (disease), and resolution from periodontal disease (resolution) ($n = 7$/group). To induce disease, ligatures were tied around the second maxillary molar for 7 days, as previously reported.[15,16] To promote resolution, ligatures were removed after the disease induction period and the animal was allowed to recover for 5 days (Figure 1A). Flow cytometry analysis of immune cells (Cd45+) infiltrating into the periodontium (the mucosa and underlying bone that support the teeth) showed that immune cells peaked in the disease group and returned to near baseline levels in the resolution group (Figure 1B). The extent of bone loss of the tooth-supporting bone is used as a clinical proxy of periodontal disease severity in mouse model.[16] Here, linear measures of the supporting maxillary bone showed that bone loss was significantly greater in the disease group compared to the others. In the resolution group, there was a significant gain in bone level compared to the disease group, but bone levels did not return to baseline and there was still significantly greater bone loss compared to control group (Figures 1C and 1D). We then used qPCR analysis to evaluate inflammatory gene expression within the periodontium. Expression of inflammatory cytokines Il-1β and Il-6 was significantly increased in the disease group compared to control. Reduction of the inflammatory genes was observed in the resolution group. Anti-inflammatory gene Il-10 remained significantly elevated in the resolution group compared to control (Figure 1E). Taken together, we validated our model of periodontal disease by showing that the resolution group was associated with bone gain and decreased inflammatory cytokine expression compared to the disease group but without a complete return to baseline conditions observed in the control group.

Single-cell RNA-sequencing identifies a heterogeneous immune cell population isolated from the oral mucosa

To understand the differential cellular immune response across the three conditions of periodontal health, disease, and resolution, we used scRNA-seq to analyze Cd45+ immune cells isolated from the periodontium of mice ($n = 3$/group). Cells were isolated via fluorescence-activated cell sorting (FACS), and single-cell library preparations were made using the 10X genomics pipeline. Sequencing was performed on an average of 2,714 cells per mouse with a mean of 202,085 reads per cell. An expanded QC analysis is presented in Figure S1. Figure 2A demonstrates the uniform manifold approximation and projection (UMAP) representation of the immune cells across all conditions. Immune cell types were assigned according to differential expression of known marker genes (Figure 2B), with each cell type demonstrating a distinct transcriptional profile (Figure 2C; Table S1). We observed a change in the proportion of immune cells isolated from the periodontium across the three conditions (Figures 2D and 2E). The disease condition was associated with an expansion of neutrophils and decrease in the proportion of B cells.

Gene signatures shift in immune cells across conditions of periodontal health, disease, and resolution

We next evaluated shifts in gene expression across the three conditions. Differential gene expression analysis was used to compare disease versus control groups and resolution versus disease groups. In this way, we were able to evaluate shifts in gene expression during the change from periodontal health to disease (disease vs. control) and during the change from periodontal disease to resolution (resolution vs. disease). Volcano plots demonstrate the significant differentially expressed genes (DEGs) globally across all cell types (p adj < 0.05) (Figure 3A). A total of 237 and 156 genes were significantly up and downregulated respectively in disease vs. control comparisons, and 192 and 416 genes were significantly up and downregulated respectively in resolution vs. disease comparisons. Inflammatory genes that have a strong association with periodontal disease pathology, such as Il-1β and TnFα, were significantly upregulated in disease vs. control and downregulated in resolution vs. disease. Similar trends were observed with genes encoding chemokines and matrix metalloproteinases. A full list of the DEGs is presented in Table S2. Figure 3B presents the DEGs by cell type. The DEGs are largely enriched within neutrophils and macrophages. In the resolution vs. disease comparison, DEGs become more apparent in B cells as well. Focusing on the DEGs in neutrophils and macrophages, a strong trend toward the upregulation of genes in disease vs. control is countered by a downregulation of genes in resolution vs. disease (Figure 3B). The heatmap in Figure 3C lists the 148 genes in neutrophils and macrophages that were conversely regulated across the two comparison groups. These 148 genes were a subset of neutrophil and macrophage DEGs presented in Figure 3B that were both upregulated in the disease vs. control comparison and downregulated in the resolution vs. disease comparison. This gene set consists of an enrichment of pro-inflammatory genes upregulated in the pathological inflammatory status of periodontal disease and then downregulated during the resolution of disease. We also observed another subset of DEGs ($n = 79$) that were only upregulated in the resolution vs. disease comparison (Figure 3D). This subset represents, in part, the transcriptional activity uniquely involved with the resolution of inflammation. Gene ontology analysis was further performed on the DEGs significantly up and downregulated in resolution vs. disease (Figure 3E). Resolution was associated with an upregulation of genes enriched for apoptotic signaling pathway and pattern recognition signaling. Genes enriched in immune response, cytokine-mediated signaling, and response to LPS were downregulated.

Gene expression shifts are associated with enriched cell-cell communication pathways across conditions

We also wanted to understand how the shift in gene expression across groups may affect cellular communication between immune cells. We performed cell-cell communication analysis using CellChat to evaluate differential enrichment of ligand-receptor gene pairs. Figure 3F presents circle plots that show the relative quantity of enriched ligand-receptor gene interactions between cell types. The thickness of the line demonstrates the quantity of potential interactions, and the red and blue color represents an increase and decrease respectively of the

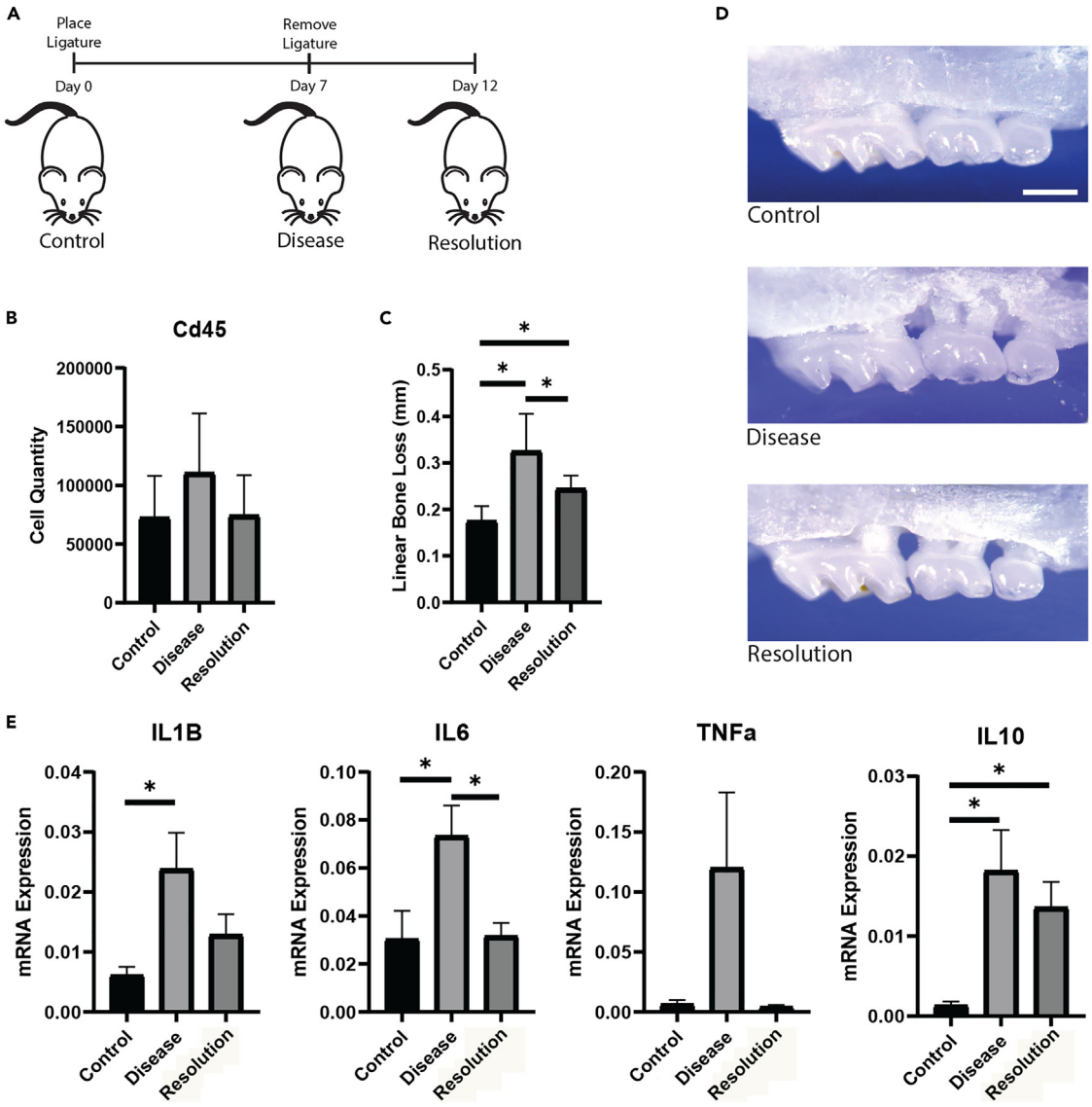

Figure 1. Validation of periodontal disease induction and resolution model

(A) A ligature model of periodontal disease was implemented in adult male mice (C57bl/6, *n* = 7/group), and mice were evaluated in conditions of control, disease, and resolution.

(B) Analysis of Cd45+ immune cells isolated from the periodontium via flow cytometry.

(C) The maxillary bone of the mice was evaluated for extent of bone loss across the three conditions.

(D) Representative photos of the maxillary process from mice of each group. Scale bar, 1 mm.

(E) qPCR analysis of gene expression within the maxillary gingival tissue from the maxilla across the three conditions. *$p < 0.05$. Data are presented at means +/- SEM.

number of interactions during disease vs. control (top) and resolution vs. disease (bottom). An increase in communication was observed between macrophages and T cells during disease compared to control conditions (thick red line). The resolution vs. disease comparison was associated with an overall decrease in cell-cell communication (blue lines), including decreased communication between macrophages and T cells. The enriched ligand-receptor gene pairs that facilitate macrophage and T cell interactions are shown in Figure 3G. The disease group is characterized by an increased number and diversity of ligand-receptor pairs compared to resolution. Macrophage interaction with T cells was shown to be facilitated through multiple ligand-receptor pairs including the macrophage inhibitory factor (Mif)-Cd74 pathway.

Expansion of an immunoregulatory macrophage subgroup is associated with the resolution of periodontal disease

We next wanted to better understand the heterogeneity within macrophages and identify potential functional subpopulations and their differential expansions across conditions. We focused our analysis on the subgroups that were identified in macrophages due to the

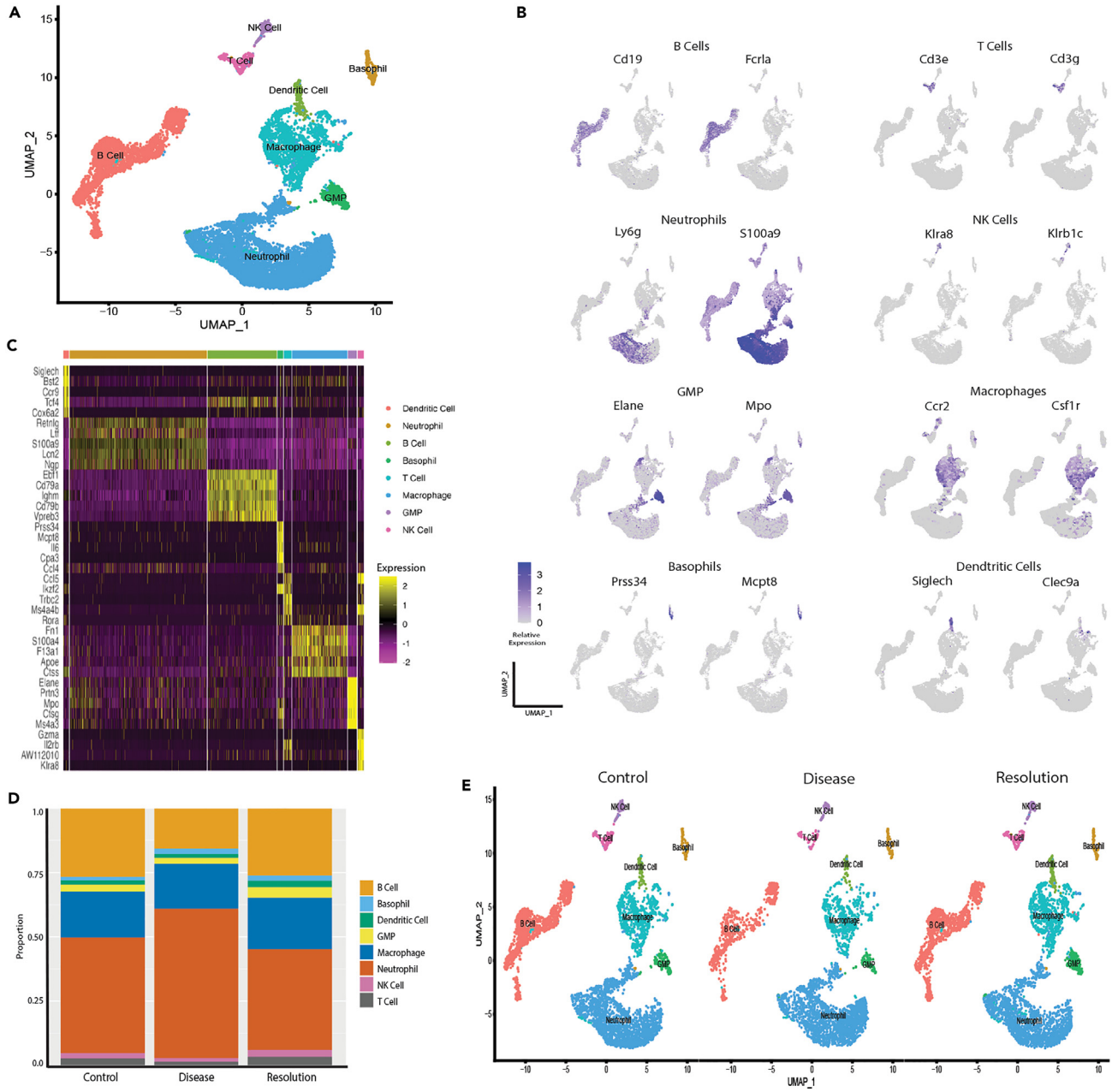

Figure 2. Single-cell RNA-sequencing identifies a heterogenous immune cell population isolated from the oral mucosa

scRNA-seq analysis was completed on immune cells (Cd45+) isolated from the periodontium of mice in three groups; controls, periodontal disease induced, and periodontal disease resolution (n = 3/group).

(A) Uniform manifold approximation and projection (UMAP) representation of the immune cells identified in the scRNA-seq analysis.

(B) Feature plots demonstrate the differential expression of characteristic cell type gene markers used to define immune cell types.

(C) Heatmap demonstrates the transcriptional differences across the defined cell types.

(D and E) Bar plot and UMAP demonstrates the change of each cell type across the three groups of periodontal control, disease, and resolution. Natural killer cells (NK Cells), granulocyte-monocyte progenitor cells (GMP).

demonstrated role of macrophage subpopulations in other conditions of health and disease.[17,18] Other subgroups were identified in this dataset within B cell and neutrophils (Table S3). Unsupervised clustering identified 4 transcriptionally distinct macrophage subgroups that shifted in proportions across control, disease, and resolution conditions (Figures 4A–4C).

We further evaluated the transcriptional profile of each subgroup to gain a better understanding of their activity (Table S3). We observed an expansion of subgroup 7 during the disease condition and demonstrated a pro-inflammatory transcriptional phenotype, including

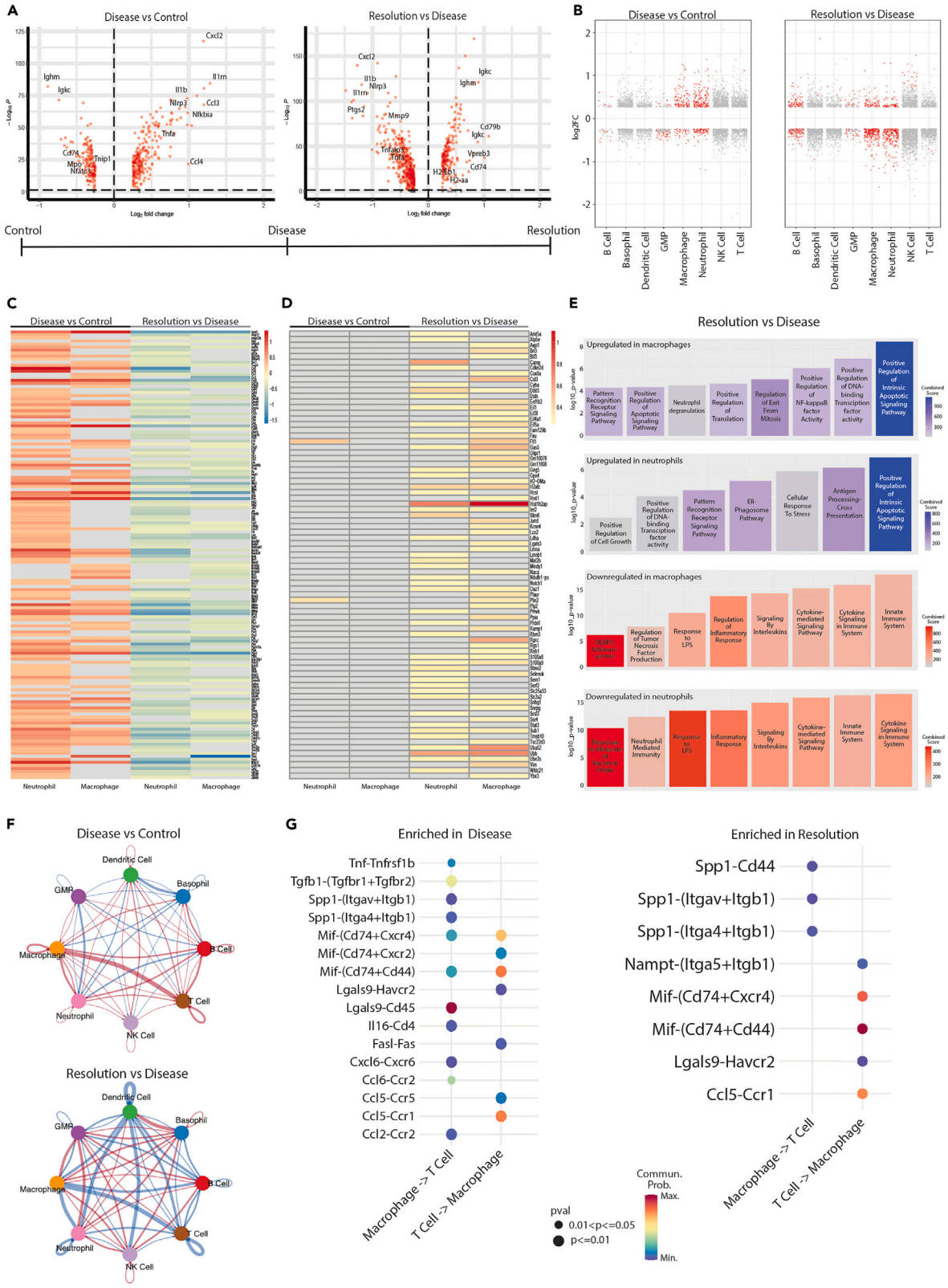
A
Disease vs Control
Resolution vs Disease
Cxcl2
Ighm
Igkc
Il1rn
Il1b
Nlrp3
Ccl3
Nfkbia
Tnfa
Cd74
Mpo
Ntrk3
Tnip1
Ccl4
Ptgs2
Mmp9
Cd79b
Vpreb3
H2-Eb1
H2-aa
Log2 fold change
Control
Disease
Resolution
B
Disease vs Control
Resolution vs Disease
log2FC
B Cell
Basophil
Dendritic Cell
GMP
Macrophage
Neutrophil
NK Cell
T Cell
C
Disease vs Control
Resolution vs Disease
Neutrophil
Macrophage
D
Disease vs Control
Resolution vs Disease
E
Resolution vs Disease
Upregulated in macrophages
Upregulated in neutrophils
Downregulated in macrophages
Downregulated in neutrophils
F
Disease vs Control
Resolution vs Disease
Dendritic Cell
Basophil
GMP
Macrophage
B Cell
T Cell
Neutrophil
NK Cell
G
Enriched in Disease
Tnf-Tnfrsf1b
Tgfb1-(Tgfbr1+Tgfbr2)
Spp1-(Itgav+Itgb1)
Spp1-(Itga4+Itgb1)
Mif-(Cd74+Cxcr4)
Mif-(Cd74+Cxcr2)
Mif-(Cd74+Cd44)
Lgals9-Havcr2
Lgals9-Cd45
Il16-Cd4
Fasl-Fas
Cxcl6-Cxcr6
Ccl6-Ccr2
Ccl5-Ccr5
Ccl5-Ccr1
Ccl2-Ccr2
Macrophage -> T Cell
T Cell -> Macrophage
Enriched in Resolution
Spp1-Cd44
Spp1-(Itgav+Itgb1)
Spp1-(Itga4+Itgb1)
Nampt-(Itga5+Itgb1)
Mif-(Cd74+Cxcr4)
Mif-(Cd74+Cd44)
Lgals9-Havcr2
Ccl5-Ccr1
Macrophage -> T Cell
T Cell -> Macrophage
Commun. Prob.
Max.
Min.
pval
0.01<p<=0.05
p<=0.01

Figure 3. Gene signature shifts identified in immune cells across control, disease, and resolution

(A) Volcano plots demonstrate the total differential gene expression in the diseased group compared to controls (left) and in the resolution group compared to the diseased group (right) (p adj < 0.05).

(B) Dot plots depict the differential gene expression by cell type in the diseased group compared to controls (left) and in the resolution group compared to the diseased group (right) (Log2FC > 0.25, p adj < 0.05).

(C) Heatmap shows the 148 genes that were inversely regulated across the two comparisons in neutrophils and macrophages.

(D) Heatmap shows the 79 genes that were only upregulated in the resolution vs. disease condition and not differentially regulated in the disease vs. control condition in neutrophils and macrophages.

(E) Gene ontology analysis was performed on the DEGs significantly up and downregulated in resolution versus disease comparisons.

(F) Gene signature shifts were also associated with differential enrichment of cell-cell communication pathways across conditions. Circle plots show the relative quantity of enriched ligand-receptor gene interactions across the immune cell types. The thickness of the line demonstrates the quantity of potential interactions. A red line represents an increase in the number of interaction within the given comparison and the blue line represents a decrease.

(G) Dot plots demonstrate the enriched ligand-receptor gene pairs that facilitate macrophage and T cell interactions in conditions of disease (left) and resolution (right).

enrichment for Mpo, Elane, Ccr2, Prtn3, and Ctsg (Figure 4B; Table S3). Subgroup 7 was also enriched with inflammatory-associated gene ontology (GO) terms including defense response to bacterium, cellular response to oxidative stress, and positive regulation of cytokine production (Figure 4D).

In contrast, subgroup 10 expanded during the resolution condition. This subgroup had a unique transcriptional profile that was enriched for GO terms that may suggest a critical role of these macrophages in the resolution of periodontal disease. These GO terms include lymphocyte chemotaxis, regulation of blood vessel remodeling, regulation of epithelial cell proliferation, and endocytosis (Figure 4D). Violin plots demonstrate the differential enrichment of immunoregulatory genes in subgroup 10 compared to the other macrophage subgroups (Figure 4E). The genes enriched within this subgroup include Tnip3, Tnfsf9, and Apoe. Tnip3 encodes TNFAIP3 interacting protein 3 which negatively regulates nuclear factor κB (NF-κB) activation and competes against TnFα, Tlr3, and Il-1β signaling to downregulate inflammation.[19,20] Tnip3 expression by macrophages has previously been demonstrated as characteristic of an anti-inflammatory macrophage response.[21] Tnfsf9 encodes the tumor necrosis factor (TNF) superfamily member 9 protein. Tnfsf9 has been shown to induce an anti-inflammatory macrophage phenotype characterized by Il-10 production.[22] Apoe expression by macrophages has been previously characterized in a select immunoregulatory subpopulation,[23] possible acting to dampen T cell activation.[24] In addition, subgroup 10 showed a significant decrease in expression of Fn1 compared to the other subgroups. High Fn1 expressing macrophages have been shown to perturb normal tissue healing and to be involved in pathologic fibrosis in kidney and heart disease and systemic sclerosis.[25,26]

Subgroup 10 was also transcriptionally defined by the significant upregulation of Cd74 expression compared to the other macrophage subgroups (Figure 4F). To validate the presence of a Cd74+ macrophage population in the periodontium, we used flow cytometry to analyze macrophages isolated from mice during control, disease, and resolution conditions (Figure 4G). Here, we validated the presence of Cd11b+, Cd74+ macrophages in the periodontium and showed that the resolution condition was associated with a significant increase in the proportion of Cd74+ macrophages compared to the disease condition (Figure 4H). Additionally, immunofluorescence was used further validates Cd74+ macrophages within the gingiva of mice in conditions of health, disease, and resolution (Figure 4I). Co-staining of Cd74 and Cd11b was identified and present in greater quantities in conditions of control and resolution.

Macrophage subgroup validation in human scRNA-seq dataset

We wanted to further understand how our findings in mice compared to immune cell profiles in human periodontal tissue during conditions of periodontal health, disease, and resolution. Toward this, we incorporated an existing human dataset that utilized scRNA-seq to analyze immune cell from periodontal tissues in patients with periodontal health, severe chronic periodontitis, or post periodontal treatment in patients with an initial diagnosis of periodontal disease.[27] We considered the post-treatment group to be comparable to our resolution model in mice. We reanalyzed this dataset applying the same analytical pipeline for our mouse dataset and replicated a similar number of distinct cell-type clusters, as presented in the original article (Figure S2A). We identified a macrophage cell cluster that showed significant overlap of expression of the macrophage marker gene used in their original analysis (C1QA) with the macrophage cell group marker used here in our mouse dataset (CSF1R) (Figures S2A–S2C). Further, we similarly identified four transcriptionally unique macrophage subclusters in the human dataset (Figures S2D and S2E; Table S4). We observed differential expansion of these macrophage subgroups across the three conditions (Figure S2F). Similarly, a resolution-associated macrophage subgroup was observed to expand during the resolution condition in the human dataset. This subpopulation also showed similar enrichment for genes involved in the immunoglobulin-mediate immune response and antigen processing (ERAP2, HLA-DOB, HLA-DPA1, HLA-DQA1, and TAP2) and endocytosis (PIK3CB, PPT1, CBL, and ARF6), similar to the processes in the resolution-associated subpopulation in our mouse models (Table S4). Finally, the resolution-associated subpopulation showed enrichment for CD74 (Figure S2G), further demonstrating the similarity in a resolution-associated macrophage population in the periodontium across human and mouse datasets.

DISCUSSION

The current study provides an immune cell dataset of the mouse oral mucosa during three distinct conditions of periodontal health, disease, and resolution. For modeling resolution, we induced periodontal disease and then allowed the mice to recover after the ligature was removed

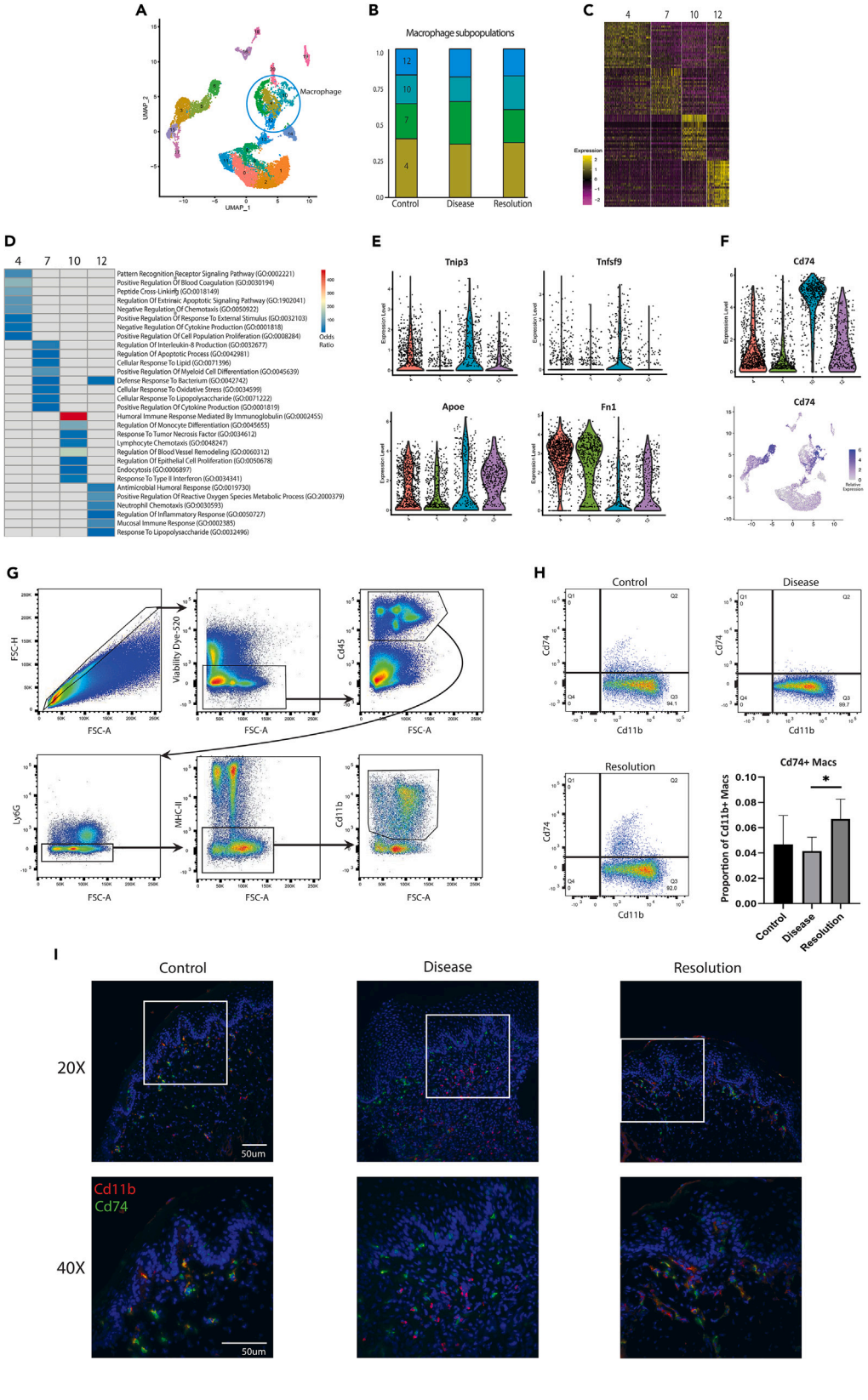
A
Macrophage
UMAP_1
UMAP_2
B
Macrophage subpopulations
Control
Disease
Resolution
C
4
7
10
12
Expression
D
4
7
10
12
Pattern Recognition Receptor Signaling Pathway (GO:0002221)
Positive Regulation Of Blood Coagulation (GO:0030194)
Peptide Cross-Linking (GO:0018149)
Regulation Of Extrinsic Apoptotic Signaling Pathway (GO:1902041)
Negative Regulation Of Chemotaxis (GO:0050922)
Positive Regulation Of Response To External Stimulus (GO:0032103)
Negative Regulation Of Cytokine Production (GO:0001818)
Positive Regulation Of Cell Population Proliferation (GO:0008284)
Regulation Of Interleukin-8 Production (GO:0032677)
Regulation Of Apoptotic Process (GO:0042981)
Cellular Response To Lipid (GO:0071396)
Positive Regulation Of Myeloid Cell Differentiation (GO:0045639)
Defense Response To Bacterium (GO:0042742)
Cellular Response To Oxidative Stress (GO:0034599)
Cellular Response To Lipopolysaccharide (GO:0071222)
Positive Regulation Of Cytokine Production (GO:0001819)
Humoral Immune Response Mediated By Immunoglobulin (GO:0002455)
Regulation Of Monocyte Differentiation (GO:0045655)
Response To Tumor Necrosis Factor (GO:0034612)
Lymphocyte Chemotaxis (GO:0048247)
Regulation Of Blood Vessel Remodeling (GO:0060312)
Regulation Of Epithelial Cell Proliferation (GO:0050678)
Endocytosis (GO:0006897)
Response To Type II Interferon (GO:0034341)
Antimicrobial Humoral Response (GO:0019730)
Positive Regulation Of Reactive Oxygen Species Metabolic Process (GO:2000379)
Neutrophil Chemotaxis (GO:0030593)
Regulation Of Inflammatory Response (GO:0050727)
Mucosal Immune Response (GO:0002385)
Response To Lipopolysaccharide (GO:0032496)
Odds Ratio
E
Tnip3
Tnfsf9
Apoe
Fn1
Expression Level
F
Cd74
Cd74
Relative Expression
G
FSC-H
FSC-A
Viability Dye-520
Cd45
Ly6G
MHC-II
Cd11b
H
Control
Disease
Resolution
Cd74
Cd11b
Q1
Q2
Q3
Q4
94.1
99.7
92.0
Cd74+ Macs
Proportion of Cd11b+ Macs
*
Control
Disease
Resolution
I
Control
Disease
Resolution
20X
40X
50um
Cd11b
Cd74

Figure 4. Expansion of an immunoregulatory macrophage subgroup is associated with the resolution of periodontal disease

(A) UMAP depicts 21 immune cell clusters identified via unsupervised clustering analysis, including four macrophage subgroups.

(B) Bar plot demonstrates the proportional shifts of each subgroup across conditions.

(C) Heatmap and (D) gene ontology demonstrate the transcriptional heterogeneity of each macrophage subgroup.

(E) Violin plots demonstrate the differential expression across all macrophage subgroups of the selected immunoregulatory genes.

(F) Violin plot and feature plot show that Cd74 expression was highly enriched in subgroup 10 compared to other macrophage subgroups. The presence of a Cd74-expressing macrophage subgroup was validated *in vivo*.

(G) Gating strategy for flow cytometry analysis used to identify Cd74+, Cd11b+ macrophages.

(H) Representative quadrant gating applied to samples in each condition (n = 7/condition) to identify Cd74+, Cd11b+ macrophages. Bar plot demonstrates the proportion of Cd74+, Cd11b+ macrophages to all Cd11b+ macrophages isolated from the periodontium of mice in control, disease, and resolution conditions.

(I) Representative immunofluorescence images of mouse gingiva stained for Cd11b (red) and Cd74 (green) in each conditions. Box within images in top row outlines ROI at higher magnification in bottom row.

*$p < 0.05$. Data are presented at means +/- SD.

for 5 days. During the recovery period, bone loss improved compared to the disease condition but did not return to baseline levels observed in the control condition (Figure 1). Similarly, inflammatory cytokine expression in the tissue decreased in the resolution group compared to disease, but not all cytokines measured returned to the baseline of the control (Figure 1). Other groups have utilized similar periodontal resolution models in mice and evaluated the extent of healing.[28,29] Wong et al. showed gains in bone levels and decreased osteoclast quantity by one week following ligature removal and a near complete return to baseline levels by 2 weeks after ligature removal.[29] Our findings here validate our model of periodontal disease resolution, as the 5-day period was sufficient to observe active resolution of disease without a complete return to baseline control conditions. Therefore, we were confident in our subsequent characterization of the transcriptional processes involved in the resolution of periodontal disease via scRNA-seq.

The shift from disease to resolution was associated with a decrease in numerous pro-inflammatory genes across macrophages and neutrophils (Figure 3). We also observed a subset of genes that was solely upregulated in the resolution condition and represented, in part, the transcriptional processes involved with the active resolution of periodontal disease (Figure 3D). Gene ontology analysis of this subset showed a significant upregulation of apoptotic signaling pathways (Figure 3E). Apoptosis of immune cells is required for the resolution of inflammation.[30,31]

Our clustering analysis demonstrated multiple cell subgroups in neutrophils, macrophages, and B cells. Interestingly, we did not observe multiple subgroups within T cells. T cell subpopulations, such as Th17 and Tregs, have been well characterized in periodontal health and disease.[32] In our analysis, T cells consisted of 2.5% of the total immune cells isolated from the periodontium. Others have similarly analyzed Cd45+ immune cells isolated from the periodontium of mice via scRNA-seq and showed a T cell fraction that was comparable[33] or markedly greater[11] to our fraction. Identifying multiple T cell clusters in our dataset may have been achieved by performing a second re-clustering analysis using a higher resolution of only T cells. However, others have found that resolving certain T cell subpopulations requires protein characterization.[34]

In addition, we observed multiple transcriptionally distinct macrophage subgroups that differentially expanded or contracted across conditions of periodontal health, disease, and resolution. Macrophages subpopulations have been identified in other tissues via scRNA-seq with described pathologic roles in the lungs[35] and kidneys[36] and having beneficial roles in bone[37] and skin healing.[38] To date, there are limited studies that have used scRNA-seq to identify macrophage subpopulations in the periodontium and describe their changes across conditions of health, disease, and resolution.

We further focused on macrophage subgroup 10, which was observed to expand during the resolution condition and demonstrated an immunoregulatory transcriptional profile with an enrichment of Tnip3, Tnfsf9, and Apoe and downregulation of Fn1. We also observed Cd74 to be significantly overexpressed in subgroup 10, and we validated Cd74 as a cell marker for this macrophage subgroup via flow cytometry and immunohistochemistry. Flow cytometry analysis showed a distinct population of Cd74+, Cd11b+ macrophages across the three conditions. The Cd74+, Cd11b+ population demonstrated a significant increase during the resolution conditions, as was also demonstrated via scRNA-seq. Cd74 is expressed on multiple cell types including B cells and macrophages,[39] as we have similarly replicated here (Figure 4F). To only quantify Cd74+ macrophages, we utilized a strict gating strategy that selected against other antigen-presenting cells (MHC-II) and neutrophils (Ly6G) (Figure 4G). Cd74 has been shown to have an important role in promoting healing and limiting inflammatory damage of heart, kidney, and lung tissue following injury or disease.[40] However, the role of Cd74 in the resolution of periodontal disease has not been previously described. Cd74 has been most prominently studied as the receptor for the macrophage migration inhibitory factor (MIF).[41] Interestingly, our cell-cell communication analysis showed a Cd74-MIF interaction mediating macrophage-T cell interactions (Figure 3G).

Limitations of the study

This study did not fully define the functional role of a Cd74+ macrophage subpopulation in the resolution of periodontal disease. Toward this, additional research is needed that incorporates *in vitro* assays that interrogate Cd74 stimulation and downstream pathway activation as well as *in vivo* experiments with Cd74 depletion and overexpression. However, we were successful in robustly validating Cd74 as a marker for a macrophage subgroup with an immunoregulatory transcriptional profile that expanded during resolution. These findings are important for future investigations that further characterize this subgroup and potentially identify therapeutics that target its expansion in the promotion of inflammatory resolution. Further, the large cell atlas generated here should provide a resourceful dataset to compare immunological changes across periodontal health, disease, and resolution.

RESOURCE AVAILABILITY

Lead contact

Further information and requests for resources and reagents should be directed to and will be fulfilled by the lead contact, Daniel Clark (Daniel.clark@pitt.edu).

Materials availability

This study did not generate new unique reagents.

Data and code availability

- The data mentioned in this paper are publicly available, and are listed in key resources table with accessibility
- The raw single cell RNA sequencing data reported in this article has been uploaded to NCBI GEO (https://www.ncbi.nlm.nih.gov/geo/) and the accession number is GSE244633.
- This paper does not report original code.
- Any additional information required to reanalyze the data reported in this paper is available from the lead contact upon request.

ACKNOWLEDGMENTS

This work is supported by National Institutes of Health grant number K08DE029505 and by the University of Pittsburgh Schools of Health Sciences funding to the Genomics Analysis Core shared resource.

AUTHOR CONTRIBUTIONS

C.P., contributed to data acquisition, analysis, and interpretation, drafted and critically revised the manuscript; D.A., P.S., C.J., and G.D. contributed to data acquisition and analysis, and critically revised the manuscript; S.V. and C.U. contributed to data acquisition, analysis, and interpretation and critically revised the manuscript. C.D. contributed to conception, design, data acquisition, analysis and interpretation, drafted and critically revised the manuscript.

DECLARATION OF INTERESTS

The authors declare no competing interest.

STAR★METHODS

Detailed methods are provided in the online version of this paper and include the following:

- KEY RESOURCES TABLE
- EXPERIMENTAL MODEL AND STUDY PARTICIPANT DETAILS
  - Periodontal disease mouse model
- METHOD DETAILS
  - Bone loss measurements
  - Quantitative real-time PCR of gingival mucosa
  - Flow cytometry
  - Immunofluorescence staining
- QUANTIFICATION AND STATISTICAL ANALYSIS
  - Single cell RNA-sequencing
  - Single cell RNA-seq analysis

SUPPLEMENTAL INFORMATION

Supplemental information can be found online at https://doi.org/10.1016/j.isci.2024.110735.

Received: January 26, 2024
Revised: June 14, 2024
Accepted: August 12, 2024
Published: August 17, 2024

REFERENCES

1. Hajishengallis, G. (2015). Periodontitis: from microbial immune subversion to systemic inflammation. Nat. Rev. Immunol. *15*, 30–44. https://doi.org/10.1038/nri3785.
2. Jiang, Q., Zhao, Y., Shui, Y., Zhou, X., Cheng, L., Ren, B., Chen, Z., and Li, M. (2021). Interactions Between Neutrophils and Periodontal Pathogens in Late-Onset Periodontitis. Front. Cell. Infect. Microbiol. *11*, 627328. https://doi.org/10.3389/fcimb.2021.627328.
3. Dutzan, N., Kajikawa, T., Abusleme, L., Greenwell-Wild, T., Zuazo, C.E., Ikeuchi, T., Brenchley, L., Abe, T., Hurabielle, C., Martin, D., et al. (2018). A dysbiotic microbiome triggers T(H)17 cells to mediate oral mucosal immunopathology in mice and humans. Sci. Transl. Med. *10*, eaat0797. https://doi.org/10.1126/scitranslmed.aat0797.
4. Cekici, A., Kantarci, A., Hasturk, H., and Van Dyke, T.E. (2014). Inflammatory and immune pathways in the pathogenesis of periodontal disease. Periodontol. *64*, 57–80. https://doi.org/10.1111/prd.12002.
5. Van Dyke, T.E., and Sima, C. (2020). Understanding resolution of inflammation in periodontal diseases: Is chronic inflammatory periodontitis a failure to resolve? Periodontol. *82*, 205–213. https://doi.org/10.1111/prd.12317.
6. Sugimoto, M.A., Sousa, L.P., Pinho, V., Perretti, M., and Teixeira, M.M. (2016). Resolution of Inflammation: What Controls Its Onset? Front. Immunol. *7*, 160. https://doi.org/10.3389/fimmu.2016.00160.
7. Serhan, C.N., Chiang, N., Dalli, J., and Levy, B.D. (2014). Lipid mediators in the resolution of inflammation. Cold Spring Harb. Perspect.

Biol. *7*, a016311. https://doi.org/10.1101/cshperspect.a016311.
8. Kantarci, A., and Van Dyke, T.E. (2005). Resolution of inflammation in periodontitis. J. Periodontol. *76*, 2168–2174. https://doi.org/10.1902/jop.2005.76.11-S.2168.
9. Sun, X., Gao, J., Meng, X., Lu, X., Zhang, L., and Chen, R. (2021). Polarized Macrophages in Periodontitis: Characteristics, Function, and Molecular Signaling. Front. Immunol. *12*, 763334. https://doi.org/10.3389/fimmu.2021.763334.
10. Qian, S.J., Huang, Q.R., Chen, R.Y., Mo, J.J., Zhou, L.Y., Zhao, Y., Li, B., and Lai, H.C. (2021). Single-Cell RNA Sequencing Identifies New Inflammation-Promoting Cell Subsets in Asian Patients With Chronic Periodontitis. Front. Immunol. *12*, 711337. https://doi.org/10.3389/fimmu.2021.711337.
11. Liu, Y., Xu, T., Jiang, W., Ma, Y., Zhang, Q., Chen, N., Chu, M., and Chen, F. (2023). Single-Cell Analyses of the Oral Mucosa Reveal Immune Cell Signatures. J. Dent. Res. *102*, 514–524. https://doi.org/10.1177/00220345221145903.
12. Davies, L.C., Jenkins, S.J., Allen, J.E., and Taylor, P.R. (2013). Tissue-resident macrophages. Nat. Immunol. *14*, 986–995. https://doi.org/10.1038/ni.2705.
13. Stables, M.J., Shah, S., Camon, E.B., Lovering, R.C., Newson, J., Bystrom, J., Farrow, S., and Gilroy, D.W. (2011). Transcriptomic analyses of murine resolution-phase macrophages. Blood *118*, e192–e208. https://doi.org/10.1182/blood-2011-04-345330.
14. Garaicoa-Pazmino, C., Fretwurst, T., Squarize, C.H., Berglundh, T., Giannobile, W.V., Larsson, L., and Castilho, R.M. (2019). Characterization of macrophage polarization in periodontal disease. J. Clin. Periodontol. *46*, 830–839. https://doi.org/10.1111/jcpe.13156.
15. Clark, D., Halpern, B., Miclau, T., Nakamura, M., Kapila, Y., and Marcucio, R. (2021). The Contribution of Macrophages in Old Mice to Periodontal Disease. J. Dent. Res. *100*, 1397–1404. https://doi.org/10.1177/00220345211009463.
16. Abe, T., and Hajishengallis, G. (2013). Optimization of the ligature-induced periodontitis model in mice. J. Immunol. Methods *394*, 49–54. https://doi.org/10.1016/j.jim.2013.05.002.
17. Sreejit, G., Fleetwood, A.J., Murphy, A.J., and Nagareddy, P.R. (2020). Origins and diversity of macrophages in health and disease. Clin. Transl. Immunology *9*, e1222. https://doi.org/10.1002/cti2.1222.
18. Wynn, T.A., and Vannella, K.M. (2016). Macrophages in Tissue Repair, Regeneration, and Fibrosis. Immunity *44*, 450–462. https://doi.org/10.1016/j.immuni.2016.02.015.
19. Verstrepen, L., Adib-Conquy, M., Kreike, M., Carpentier, I., Adrie, C., Cavaillon, J.M., and Beyaert, R. (2008). Expression of the NF-kappaB inhibitor ABIN-3 in response to TNF and toll-like receptor 4 stimulation is itself regulated by NF-kappaB. J. Cell Mol. Med. *12*, 316–329. https://doi.org/10.1111/j.1582-4934.2007.00187.x.
20. Wullaert, A., Verstrepen, L., Van Huffel, S., Adib-Conquy, M., Cornelis, S., Kreike, M., Haegman, M., El Bakkouri, K., Sanders, M., Verhelst, K., et al. (2007). LIND/ABIN-3 is a novel lipopolysaccharide-inducible inhibitor of NF-kappaB activation. J. Biol. Chem. *282*, 81–90. https://doi.org/10.1074/jbc.M607481200.
21. Hutchins, A.P., Poulain, S., and Miranda-Saavedra, D. (2012). Genome-wide analysis of STAT3 binding in vivo predicts effectors of the anti-inflammatory response in macrophages. Blood *119*, e110–e119. https://doi.org/10.1182/blood-2011-09-381483.
22. Wu, J., Wang, Y., Yang, Y., Liu, F., Chen, J., Jiang, Z., and Jiang, Z. (2021). TNFSF9 promotes metastasis of pancreatic cancer through Wnt/Snail signaling and M2 polarization of macrophages. Aging (Albany NY) *13*, 21571–21586. https://doi.org/10.18632/aging.203497.
23. Baitsch, D., Bock, H.H., Engel, T., Telgmann, R., Müller-Tidow, C., Varga, G., Bot, M., Herz, J., Robenek, H., von Eckardstein, A., and Nofer, J.R. (2011). Apolipoprotein E induces antiinflammatory phenotype in macrophages. Arterioscler. Thromb. Vasc. Biol. *31*, 1160–1168. https://doi.org/10.1161/ATVBAHA.111.222745.
24. Tenger, C., and Zhou, X. (2003). Apolipoprotein E modulates immune activation by acting on the antigen-presenting cell. Immunology *109*, 392–397. https://doi.org/10.1046/j.1365-2567.2003.01665.x.
25. Rudnik, M., Hukara, A., Kocherova, I., Jordan, S., Schniering, J., Milleret, V., Ehrbar, M., Klingel, K., Feghali-Bostwick, C., Distler, O., et al. (2021). Elevated Fibronectin Levels in Profibrotic CD14(+) Monocytes and CD14(+) Macrophages in Systemic Sclerosis. Front. Immunol. *12*, 642891. https://doi.org/10.3389/fimmu.2021.642891.
26. Hoeft, K., Schaefer, G.J.L., Kim, H., Schumacher, D., Bleckwehl, T., Long, Q., Klinkhammer, B.M., Peisker, F., Koch, L., Nagai, J., et al. (2023). Platelet-instructed SPP1(+) macrophages drive myofibroblast activation in fibrosis in a CXCL4-dependent manner. Cell Rep. *42*, 112131. https://doi.org/10.1016/j.celrep.2023.112131.
27. Chen, Y., Wang, H., Yang, Q., Zhao, W., Chen, Y., Ni, Q., Li, W., Shi, J., Zhang, W., Li, L., et al. (2022). Single-cell RNA landscape of the osteoimmunology microenvironment in periodontitis. Theranostics *12*, 1074–1096. https://doi.org/10.7150/thno.65694.
28. Ishii, T., Ruiz-Torruella, M., Yamamoto, K., Yamaguchi, T., Heidari, A., Pierrelus, R., Leon, E., Shindo, S., Rawas-Qalaji, M., Pastore, M.R., et al. (2022). Locally Secreted Semaphorin 4D Is Engaged in Both Pathogenic Bone Resorption and Retarded Bone Regeneration in a Ligature-Induced Mouse Model of Periodontitis. Int. J. Mol. Sci. *23*, 5630. https://doi.org/10.3390/ijms23105630.
29. Wong, R.L., Hiyari, S., Yaghsezian, A., Davar, M., Lin, Y.L., Galvan, M., Tetradis, S., Camargo, P.M., and Pirih, F.Q. (2017). Comparing the Healing Potential of Late-Stage Periodontitis and Peri-Implantitis. J. Oral Implantol. *43*, 437–445. https://doi.org/10.1563/aaid-joi-D-17-00157.
30. Greenlee-Wacker, M.C. (2016). Clearance of apoptotic neutrophils and resolution of inflammation. Immunol. Rev. *273*, 357–370. https://doi.org/10.1111/imr.12453.
31. Haanen, C., and Vermes, I. (1995). Apoptosis and inflammation. Mediators Inflamm. *4*, 5–15. https://doi.org/10.1155/S0962935195000020.
32. Figueredo, C.M., Lira-Junior, R., and Love, R.M. (2019). T and B Cells in Periodontal Disease: New Functions in A Complex Scenario. Int. J. Mol. Sci. *20*, 3949. https://doi.org/10.3390/ijms20163949.
33. Wang, Q., Lin, W., Zhou, X., Lei, K., Xu, R., Zhang, X., Xiong, Q., Sheng, R., Song, W., Liu, W., et al. (2022). Single-Cell Transcriptomic Atlas of Gingival Mucosa in Type 2 Diabetes. J. Dent. Res. *101*, 1654–1664. https://doi.org/10.1177/00220345221092752.
34. Hao, Y., Hao, S., Andersen-Nissen, E., Mauck, W.M., 3rd, Zheng, S., Butler, A., Lee, M.J., Wilk, A.J., Darby, C., Zager, M., et al. (2021). Integrated analysis of multimodal single-cell data. Cell *184*, 3573–3587.e29. https://doi.org/10.1016/j.cell.2021.04.048.
35. Mould, K.J., Jackson, N.D., Henson, P.M., Seibold, M., and Janssen, W.J. (2019). Single cell RNA sequencing identifies unique inflammatory airspace macrophage subsets. JCI Insight *4*, e126556. https://doi.org/10.1172/jci.insight.126556.
36. Yao, W., Chen, Y., Li, Z., Ji, J., You, A., Jin, S., Ma, Y., Zhao, Y., Wang, J., Qu, L., et al. (2022). Single Cell RNA Sequencing Identifies a Unique Inflammatory Macrophage Subset as a Druggable Target for Alleviating Acute Kidney Injury. Adv. Sci. *9*, e2103675. https://doi.org/10.1002/advs.202103675.
37. Li, J., Zhao, C., Xu, Y., Song, L., Chen, Y., Xu, Y., Ma, Y., Wang, S., Xu, A., and He, F. (2023). Remodeling of the osteoimmune microenvironment after biomaterials implantation in murine tibia: Single-cell transcriptome analysis. Bioact. Mater. *22*, 404–422. https://doi.org/10.1016/j.bioactmat.2022.10.009.
38. Henn, D., Chen, K., Fehlmann, T., Trotsyuk, A.A., Sivaraj, D., Maan, Z.N., Bonham, C.A., Jr., Barrera, J.A., Mays, C.J., Greco, A.H., et al. (2021). Xenogeneic skin transplantation promotes angiogenesis and tissue regeneration through activated Trem2(+) macrophages. Sci. Adv. *7*, eabi4528. https://doi.org/10.1126/sciadv.abi4528.
39. Zheng, Y.X., Yang, M., Rong, T.T., Yuan, X.L., Ma, Y.H., Wang, Z.H., Shen, L.S., and Cui, L. (2012). CD74 and macrophage migration inhibitory factor as therapeutic targets in gastric cancer. World J. Gastroenterol. *18*, 2253–2261. https://doi.org/10.3748/wjg.v18.i18.2253.
40. Farr, L., Ghosh, S., and Moonah, S. (2020). Role of MIF Cytokine/CD74 Receptor Pathway in Protecting Against Injury and Promoting Repair. Front. Immunol. *11*, 1273. https://doi.org/10.3389/fimmu.2020.01273.
41. Leng, L., Metz, C.N., Fang, Y., Xu, J., Donnelly, S., Baugh, J., Delohery, T., Chen, Y., Mitchell, R.A., and Bucala, R. (2003). MIF signal transduction initiated by binding to CD74. J. Exp. Med. *197*, 1467–1476. https://doi.org/10.1084/jem.20030286.
42. Jin, S., Guerrero-Juarez, C.F., Zhang, L., Chang, I., Ramos, R., Kuan, C.H., Myung, P., Plikus, M.V., and Nie, Q. (2021). Inference and analysis of cell-cell communication using CellChat. Nat. Commun. *12*, 1088. https://doi.org/10.1038/s41467-021-21246-9.

STAR★METHODS

KEY RESOURCES TABLE

REAGENT or RESOURCE	SOURCE	IDENTIFIER
Antibodies		
Rat anti-Cd45	BD Biosciences	Cat#553076; RRID: AB_394606
Rat anti-MHC Cl II	BD Biosciences	Cat#556999; RRID: AB_396545
Rat anti-Ly6C	BD Biosciences	Cat#560595; RRID: AB_1727554
Rat anti-Ly6G	BD Biosciences	Cat#551459; RRID: AB_394206
Rat anti-F480	BD Biosciences	Cat#565409; RRID: AB_2739222
Rat anti-Cd11b	BD Biosciences	Cat#550282; RRID: AB_393577
Rat anti-Cd74	R&D Systems	Cat#FAB7478; RRID: AB_3137121
Rat anti-Cd11b	Invitrogen	Cat#MA180091; RRID: AB_927467
Rabbit anti-Cd74	abcam	Cat#ab245692; RRID: AB_2924345
Goat anti-rat Alexa Fluor 546	Invitrogen	Cat#A-11081; RRID: AB_2534125
Goat anti-rabbit Alexa Fluor 488	Invitrogen	Cat#A-11034; RRID: AB_2576217
Critical commercial assays		
PowerUp SYBR Green Master Mix for qPCR	Applied Biosystems	Cat# A25776
SuperScript™ III Reverse Transcriptase	Invitrogen	Cat#18080093
Deposited data		
Single-cell RNA sequencing data	This paper	NCBI Geo: GSE244633
Single-cell RNA sequencing data	Chen et al.[27]	NCBI Geo: GSE171213
Oligonucleotides		
qPCR Primers	IDT	See Table S5
Software and algorithms		
GraphPad Prism 10	GraphPad Software	NA
Fiji	ImagJ	https://imagej.net/Fiji/Downloads
Adibe Illustrator	Adobe	https://www.adobe.com/products/illustrator.html
RStudio	RStudio	https://www.rstudio.com/products/rstudio/download/

EXPERIMENTAL MODEL AND STUDY PARTICIPANT DETAILS

Periodontal disease mouse model

The animal procedures were approved by the University of Pittsburgh Institutional Animal Care and Use Committee and were performed in accordance with the guidelines of the US National Institutes of Health for the care and use of laboratory animals and the ARRIVE checklist. Male C57BL/6 mice were used for all experiments at the age of 4 months. Three groups of mice were compared in each analysis: healthy controls (control), periodontal disease induction (disease), and periodontal disease resolution (resolution). Periodontal disease was induced using the ligature method as described previously.[15] Mice were first anesthetized with an intraperitoneal injection of a 1:1 solution of dexmedetomidine and ketamine. A 6.0 silk suture was tied in a subgingival position around the second maxillary molars bilaterally. The sutures remained in place for 7 days to induce a local osteolytic inflammatory response and characteristic periodontal disease phenotype. In the disease group, mice were euthanized after 7 days and tissues were isolated for analysis. In the resolution group, the ligature was removed after 7 days, and mice were allowed to recover for an additional 5 days before they were euthanized.

METHOD DETAILS

Bone loss measurements

Periodontal disease severity was evaluated by quantifying the extent of linear bone loss in the maxilla of mice. Mice from control, disease, and resolution groups were compared (n = 7/group). One-half of the maxilla containing the 3 M teeth was isolated, defleshed, and placed in 30% hydrogen peroxide overnight, and then fixed in 70% ethanol. Magnified images of the maxilla were captured using a dissecting microscope (Leica M165 FC, Leica Microsystems Ltd). One image of the buccal aspect and one image of the palatal aspect of the maxilla were captured for

each sample. Measurement calibrations were made possible by including a ruler in each image placed adjacent to the sample. Linear bone loss was measured from the cementoenamel junction (CEJ) to the bone crest (ABC) at 6 sites per tooth (3 sites on the buccal and 3 sites on the palatal surface of each tooth). Bone loss measurements were made on the images using ImageJ. All measurement sites were averaged per animal.

Quantitative real-time PCR of gingival mucosa

The extent of inflammation locally in the gingiva of the mice was evaluated by quantifying inflammatory cytokine gene expression via quantitative real-time PCR (qRT-PCR). Mice from control, disease, and resolution groups were compared (n = 7/group). Gingiva was isolated from one-half of the maxilla. The isolated gingiva was prepared for qRT-PCR analysis. Briefly, gingiva was homogenized in Trizol and RNA was isolated. cDNA was reverse transcribed using Superscript III (Invitrogen). qRT-PCR was performed with SYBR Green. See Table S5 for list of primers.

Flow cytometry

Both halves of the maxilla were isolated from mice in the control, disease, and resolution groups (n = 6/group). Maxilla were disassociated manually and then stravm ined using a 100 μm cell strainer. Tissues was further digested with collagenase type 1 (0.2 mg/mL, Worthington Lakewood, NJ) for 1 h at 37°C. Cells were washed, collected by centrifugation, and resuspended in incubation buffer (0.5% BSA in PBS). Isolated cells were blocked for 10 min in 10% rat serum. To detect dead cell, cells were stained with Fixable Viability Dye (BD Biosciences Franklin Lakes, NJ). Cell were also stained with directly conjugated fluorescent antibodies (Rat anti-mouse): CD45 (clone 30-F11), MHC Class II (M5/114.15.2), Ly6C (AL21), Ly6G (clone 1A8), F4/80 (T45-2342), CD11b (clone M1/70) (BD Biosciences, Franklin Lakes, NJ), and Cd74 (clone 829706) (R&D Systems, Minneapolis, MN). Fluorescence minus one controls were used to gate for background staining. Cells were analyzed and/or sorted on a FACSAria (BD Biosciences, San Jose, CA). FlowJo Software 9.6 (Treestar, Ashland, OR) was used for analysis.

Immunofluorescence staining

Gingiva from one-half of the maxilla was isolated and flash frozen and −80°C. Samples were embedded in optimal cutting temperature compound (Tissue-Tek; Sakura Finetek). Frozen serial sections were cut at a thickness of 10 μm. Frozen sections were fixed on the slide with 100% ethanol for 15 min. Next, sections were blocked in 5% goat serum for 1 h and then incubated with the primary antibodies overnight at 4°C, Rat anti-mouse Cd11b (1:25) (MA1-80091, Invitrogen)) and rabbit anti-mouse Cd74 (1:1000) (ab245692, abcam). After rinsing with PBS-T, fluorescent conjugated secondary antibodies were applied to each section for 2 h, goat anti-rat Alexa Fluor 546 (1:100) (Invitrogen) and goat anti-rabbit Alexa Fluor 488 (1:400) (Invitrogen). DAPI (Invitrogen) was applied at (1:1000). Slides were then mounted and representative images were captured at 20× and 40× using a Nikon fluorescence microscope.

QUANTIFICATION AND STATISTICAL ANALYSIS

The linear bone loss and cell quantification were calculated per sample and presented as mean ± standard deviation (SD). Analysis of variance (ANOVA) was utilized to first test for significant differences across all groups. Further, between-group differences were analyzed using a 2-tailed t test. Quantitative real-time PCR (qRT-PCR) used technical triplicates and the mean QT value was calculated. mRNA expression (2^- ΔCT) was calculated and presented as mean ± standard error of the mean (SEM) and analyzed using an ANOVA followed by between-group comparisons using a 2-tailed t test. Significance for all analysis was determined at $p < 0.05$. All statistical analysis was performed using GraphPad Prism v.7 software (GraphPad Software, Inc.).

Single cell RNA-sequencing

Cells were isolated from the periodontium of mice in control, disease, and resolution conditions (n = 3/group). Viable $CD45^+$ cells were isolated via flow cytometry as described above. The isolated cells were prepared in a single cell suspension and library preparation was performed using the Chromium Single Cell 3′ Reagent Version 3 Kit (10× Genomics). Each sample was loaded and run on separate lanes. Droplets were subjected to reverse transcription and then cDNA amplified. The prepared libraries were sequenced on an Illumina HiSeq4000. The mouse reference genome, mm 10, was downloaded from 10× Genomics (https://cf.10xgenomics.com/supp/cell-exp/refdata-gex-mm10-2020-A.tar.gz). Raw reads were processed using the reference genome with Cell Ranger (v6.1) to generate raw UMI count tables.

Single cell RNA-seq analysis

Seurat version 4 was used for analysis.[34] The percentage of mitochondrial reads per cell was determined using PercentageFeatureSet. Then, cells were removed according to the following metrics: <300 features expressed, UMI counts <1,000 or >50,000, or >10% mitochondrial reads. Genes were removed that were not expressed in at least 3 cells. After filtering, the number of cells remaining ranged from 892 to 2453 and the number of genes remaining was 20,416. The raw UMI counts were normalized using NormalizeData. The Seurat 'cc.genes.updated.2019' human gene symbols were converted to mouse symbols using the homologene R package and subsequently used to determine the cell cycle phase of each cell with CellCycleScoring. Then, variable genes (HVG) were determined using the 'vst' method. To determine cell cycle associated HVGs, we used getVarianceExplained from the R package scater which identified 294 genes that we removed from the HVG list (1706 HVGs remained). Then the HVGs were scaled with regression on 'nCount_RNA' and used to determine a PCA. We determined the number of

PCA dimensions to use by identifying the PCs accounting for 75% of the cumulative PCA standard deviation (PCs 1 to 29). These PCs were used to generate a UMAP using RunUMAP and clusters were determined with FindClusters using default parameters.

Subclustering

The expression of immune cell type markers was visualized with FeaturePlot and used to annotate cell types to each cluster. Three clusters were removed without transcriptional signatures of known immune cell types. Seurat was used to analyze and recluster the remaining cells (ranging from 856 to 2396 cells per sample) similar to the methods above. Briefly, 326 HVGs were found to be associated with the cell cycle and removed (1674 HVGs remained). After scaling and PCA, the first 29 PCs were used to generate a UMAP and determine cell clusters.

Markers

Cell type markers were determined using FindAllMarkers. Differentially expressed genes between conditions per cell type or across all cells (aka. global) was determined using FindMarkers. The defaults were used for the two functions except that the 'min.pct' parameter was increased to 0.25. Heatmaps of the top 5 or 25 genes were generated with DoHeatmap. To generate volcano and boxplots, cell type markers and global DEG were filtered to remove ribosomal genes.

Gene ontology analysis

The resolution vs. disease differentially expressed genes for Macrophages and Neutrophils were filtered to remove ribosomal genes and on adjusted P-value <0.05 to obtain lists of significantly up and downregulated genes. These gene lists were uploaded to Enrichr (https://maayanlab.cloud/Enrichr/) to obtain the GO Biological Process 2023 regulated pathways. Barplots were generated with ggplot2 using the -log10(P-value) and colored by combined score.

CellChat

CellChat version 1.6.1 was used to infer cell-cell communication between cell types.[42] The CellChat vignette for a single dataset was followed to generate a CellChat object for each condition (control, disease, and resolution) using the "Secreted Signaling" subset of the mouse database. To compare two conditions, we used the multi-sample vignette. A circle plot was generated using netVisual_diffInteraction to show the differential number of interactions between cell populations. Bubble plots were created using netVisual_bubble to show the upregulated ligand-receptor pairs between two conditions.

Data visualizations

Several R packages were used to generate plots. Volcano plots were built using EnhancedVolcano (v.1.16.0), heatmaps were generated using pheatmap (v1.0.12) and ggplot2 (v3.3.6) was used to generate boxplots and percent stacked barplots.